Spatial Reconstruction of Soil Moisture Content using Non-Contact Thermoacoustic Imaging

Aidan Fitzpatrick, Ajay Singhvi, and Amin Arbabian
Department of Electrical Engineering, Stanford University, Stanford, CA, USA

***Abstract*—Sensing of soil water content is useful in many precision agriculture and resource management applications, particularly if the sensing technique permits frequent field-scale measurements at depth. To date, soil moisture sensing technologies have a trade-off between point based measurements at depth or rapid, remote measurements of water content near the surface. In this paper, we propose a non-contact thermoacoustic soil moisture sensing modality which could permit high-resolution, high-throughput mapping of water content at depth. Within, we develop an algorithm for reconstructing the speed-of-sound in soil, which is known to be highly correlated with the soil moisture content. Through verification in simulation, our algorithm demonstrates high fidelity – reconstructing speed-of-sound profiles that match well with the ground-truth.**

***Index Terms*—below-ground sensing, capacitive micromachined ultrasonic transducer, CMUT, soil moisture, speed-of-sound reconstruction, thermoacoustics, ultrasound**

I. Introduction

Soil moisture sensing has numerous applications due to its influence on hydrological, geological, biological, ecological, and agronomic functions of the soil mass [1]. Point based, in-situ soil moisture sensors [2]–[5] provide accurate information across depths but are limited by their spatial coverage. Remote sensing has enabled non-destructive mapping of soil moisture near the surface on a continental scale [6], but does not provide information about moisture content deeper in the soil.

There is a dearth of tools that provide soil moisture information at depth, while being deployed on an intermediate spatial scale [7] in a non-invasive fashion. Such tools could provide measurements of heterogeneity in soil moisture profiles across field sites and be useful for many precision agriculture and resource management applications. These soil moisture profiles could also be used as indicators of root presence and root water uptake [8], and be deployed to study root hydrotropism [9] and hydropatterning [10] responses. Thus, in addition to existing applications, such a technology also addresses challenges of studying the interaction between the root-system architecture and the rhizosphere in field conditions by providing large quantities of relevant data over time [11].

Ground Penetrating Radar (GPR) [12], [13] has been proposed as a viable approach for such soil moisture mapping, but GPR systems have a fundamental tradeoff between resolution and penetration depth through the GPR frequency, and can only operate reliably in regions with electrically resistive soil [14].

This work was supported by an Advanced Research Projects Agency-Energy Grant: DE-AR0000825, sponsored by the ROOTS program.

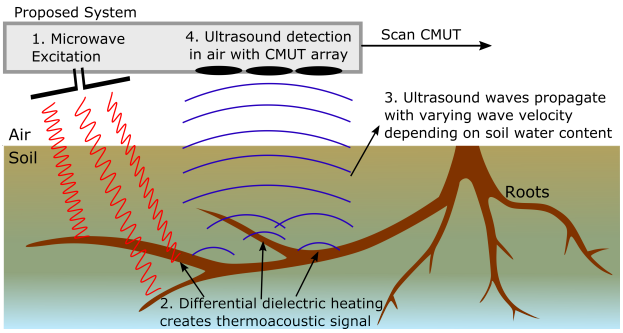

Fig. 1. Conceptual view of proposed non-contact thermoacoustic soil moisture sensing system

To overcome these challenges, we propose a non-contact thermoacoustic (NCTA) soil moisture sensing modality that can also augment earlier experimental demonstrations of a NCTA system used for below-ground imaging [11], [15]. It is a multi-modal sensing approach that combines high microwave contrast with good ultrasound (US) resolution. By decoupling the transmit and receive mechanisms, this hybrid approach overcomes the limitations of GPR based methods to provide spatial soil moisture profiles and their variation with depth, with improved resolution across different soil types. The use of highly sensitive, air-coupled capacitive micromachined ultrasound transducers (CMUT) [16] allows for non-contact, autonomous operation permitting high-throughput, dynamic measurements over large areas.

II. Thermoacoustic Soil Moisture Sensing

Fig. 1 shows a conceptual view of the NCTA sensing system. A microwave excitation source modulated at the desired US frequency irradiates the soil and roots. Difference in dielectric properties between the soil and roots results in differential heating at the soil-root interface which in turn causes the generation of an US signal via the thermoacoustic (TA) effect. This generated signal propagates through the soil, then passes through the soil-air interface and is captured using an array of CMUT receivers present at a standoff in air. Additional system details can be found in [15].

Experimental studies have shown that the propagation velocity of US waves in soil depends on the soil moisture content and water potential [11], [17], [18]. Given the correlation between the speed-of-sound (SoS) and soil moisture content, a reconstructed SoS distribution could be used to extrapolate soil moisture profiles. Thus, in this preliminary work we propose a novel SoS reconstruction algorithm for use in our NCTA system and verify the performance of the technique through

978-1-7281-6801-2/20/$31.00 ©2020 IEEE

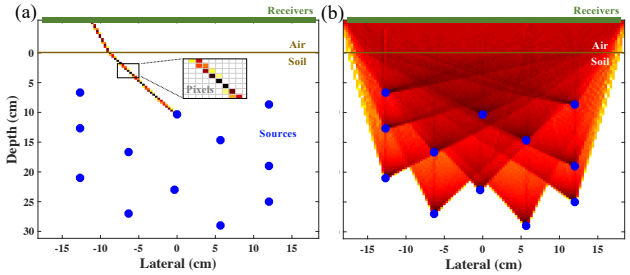

Fig. 2. (a) Single acoustic ray path from source to receiver and (b) acoustic ray paths for all source-receiver pairs.

a simulation framework. Experiments in the field are beyond the scope of this paper and will be addressed in future work.

III. Speed-of-Sound Reconstruction Algorithm

Reconstruction of the SoS, which we use as a proxy for the soil moisture content, has been explored in medical US imaging for phase aberration correction and for diagnostics [19]–[24]. The general theme for these approaches is to find the spatial SoS distribution which satisfies the equation:

$$\mathbf{t} = \boldsymbol{H}(s)\mathbf{s}, \tag{1}$$

where $\mathbf{t}$ is a vector containing the empirical time-of-flight (ToF) of US signals, $\mathbf{s}$ is the vectorized slowness distribution or equivalently $\frac{1}{SoS}$ defined at each pixel in the discretized image domain, and $\boldsymbol{H}(s)$ is a forward model matrix which encodes integration of the slowness distribution along the acoustic paths traversed by the US signals. The matrix-vector product $\boldsymbol{H}(s)\mathbf{s}$ represents the algorithmically calculated ToFs, while $\mathbf{t}$ represents the experimentally captured ToFs. The calculated ToFs converge to the captured ToFs when we have an accurate estimate of the SoS distribution. The algorithm presented here exploits similar concepts to previous works by formulating the SoS reconstruction using NCTA imaging as an inverse problem in the form of (1).

A. Empirical Time-of-Flight $\mathbf{t}$

Whereas in some applications transducer-to-transducer US signals can be transmitted through the medium of interest to determine the ToF along a path, the imaging geometry here does not permit tomographic approaches with an enclosing transducer array [21]–[24]. Instead, our approach relies on underground structures which can be excited via the TA effect to act as in-soil US transmitters.

In this paper, we model TA sources as discrete, artificially introduced sources, though future work will aim to exploit existing root systems, other buried structures, or inherent underground heterogeneity [13]. As with tomography, the number of projections and their angular diversity through the medium of interest is important to obtaining a well-posed inverse problem [25]. In our application, this requires TA sources at varying depths in the soil. We expect this to be true in realistic underground environments with sufficient heterogeneity; however, for our discrete source formulation, we use a scattered source placement as shown as the blue circles in Fig. 2(a). Fig. 2(b) shows sufficient diversity of the acoustic paths through the soil between all of the source-receiver pairs that prevent the problem from being severely ill-posed.

When the sources are excited with microwave energy, the US signals emit from all sources simultaneously. As a result, it is not possible to isolate ToF information of each individual source's US signal from the captured data without further processing. To estimate ToF of US signals along acoustic paths for each source-receiver pair, we discretize the soil medium into image pixels and use the coherence factor (CF) formalism [26]:

$$CF_i = \frac{|\sum_{k=1}^{N} s_k[i]|^2}{N\sum_{k=1}^{N}|s_k[i]|^2}, \tag{2}$$

where CF_i is the CF defined at image pixel i, N is the number of receivers, and $s_k[i]$ is the signal received at receiver k sampled at the ToF that corresponds to pixel i for the assumed SoS distribution.

The CF is highest when the assumed SoS distribution results in proper focusing of the received US signals to a given location in soil. Therefore, by looping over uniform SoS values for the soil, the SoS which maximizes the CF at each source location can be used to estimate the ToF for every source-receiver pair [27]. Despite the fact that the soil SoS distribution is not truly uniform, this approach finds an average SoS to the source location that can be used to determine the empirical ToF with a straight ray path assumption in the soil. This assumption is fairly robust as long as the true SoS distribution does not have large lateral variations. The SoS in air is held constant at 340 m/s [28] and thus refraction at the air-soil interface and height of receivers must also be considered. These empirical ToFs are stored in the vector $\mathbf{t}$; if there are M sources, $\mathbf{t} \in \mathbb{R}^{MN}$.

B. Constructing Forward Model $\boldsymbol{H}$

After extracting the empirical ToF data, we must construct the forward model matrix $\boldsymbol{H}$ before solving the inverse problem in (1). Here, and for the remainder of this paper, we discuss two-dimensional acoustic propagation, though the methods applied could be scaled to three-dimensional geometries. The two-dimensional Eikonal equation is written as:

$$\sqrt{\left(\frac{\partial\tau}{\partial x}\right)^2 + \left(\frac{\partial\tau}{\partial z}\right)^2} = s(x,z), \tag{3}$$

This equation relates the slowness distribution $s(x,z)$ to the time accumulation along the propagation path while inherently considering refraction. This nonlinear partial differential equation can be solved efficiently using the Fast Marching Method (FMM) [29]. The solution attained via the FMM solves for the ToF from each pixel location to a receiver location, producing a ToF map as depicted in Fig. 3 for each of the N receivers.

By tracing the steepest gradient from a source location through each of the ToF maps, the acoustic path can be found for every source-receiver pair. An example output of the gradient descent ray tracing is shown in Fig. 2, where (a)

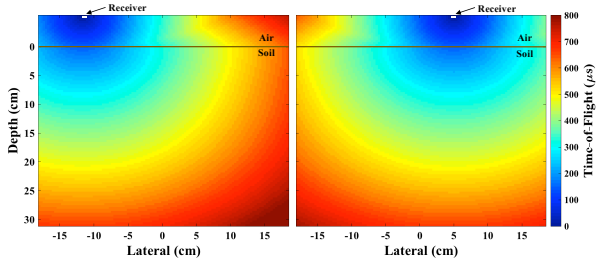

Fig. 3. FMM-generated ToF maps for two different receivers.

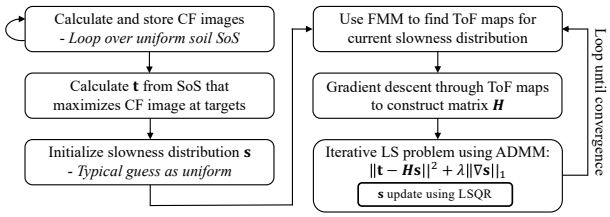

Fig. 4. Reconstruction algorithm for spatial distribution of SoS. The first step loops over typical SoS range for US in soil [18]

shows a single acoustic path and (b) shows all of the acoustic paths. The matrix $\boldsymbol{H}(s)$ is constructed such that each row encodes the pixels along a single acoustic path through the slowness distribution. If the slowness distribution is defined over X lateral pixels and Z depth pixels, $\boldsymbol{H} \in \mathbb{R}^{MN \times XZ}$.

C. Iterative Least Squares Solution for s

In the construction of the matrix $\boldsymbol{H}(s)$, the acoustic paths are dependent on the slowness distribution, thus resulting in the inverse problem in (1) being nonlinear. In addition, the inverse problem is clearly ill-conditioned due to some pixels in the domain not being intersected by acoustic paths as seen in Fig. 2(b). Therefore, we use a total variation (TV) regularization which penalizes SoS distributions with high gradients:

$$\hat{\mathbf{s}} = \arg\min_{\mathbf{s}} ||\mathbf{t} - \boldsymbol{H}(s)\mathbf{s}||^2 + \lambda ||\nabla \mathbf{s}||_1, \tag{4}$$

where λ is the regularization parameter, $||\cdot||$ is the 2-norm, and $||\cdot||_1$ is the 1-norm. We solve this regularized least-squares problem iteratively using Alternating Direction Method of Multipliers (ADMM) which enables decoupling of the objectives into two independent problems [30]. The iterative approach removes the nonlinear dependence on the slowness distribution such that each iteration involves solving a linear problem and permits the use of the efficient LSQR method for updating the distribution [31]. After convergence, the slowness distribution is pixel-wise inverted to find the reconstructed SoS distribution. The algorithm is summarized in Fig. 4.

IV. Simulation Results

We implement the algorithm described in Section III in MATLAB and test its efficacy on data collected through acoustic simulations using the k-Wave toolbox [32]. The k-Wave simulation setup consists of scattered acoustic sources embedded in the soil medium as depicted by the blue circles in Fig. 2(a); again, in a practical use case these sources would be excited via the TA effect as shown in Fig. 1. The ground-truth

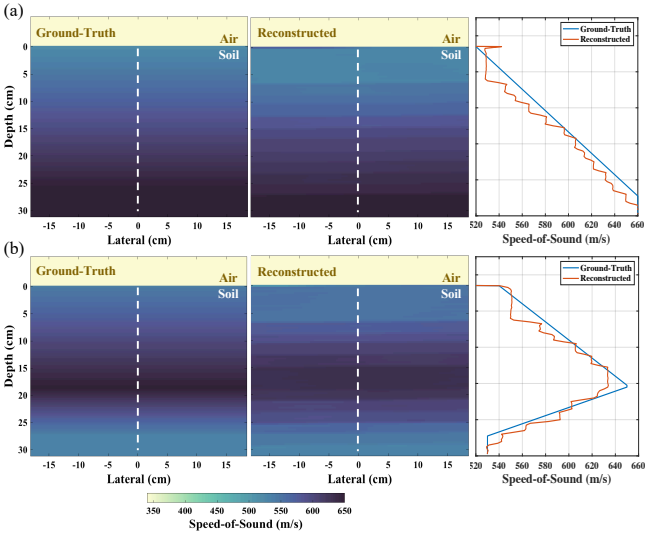

Fig. 5. Left: Ground-truth, Middle: Reconstructed, Right: Slice through profiles noted by dashed lines for (a) monotonic and (b) non-monotonic SoS profiles. RMS errors of (a) 9.7 m/s and (b) 10 m/s.

SoS distributions are shown in the left column of Fig. 5; these were chosen to validate the algorithm's robustness to both monotonic and non-monotonic distributions. The receivers are modeled in the simulation as uniformly $\lambda/2$-spaced point detectors that are 5 cm above the soil interface. For these simulations we assume the use of our previously reported CMUTs as receivers, which have a 71 kHz center frequency and a 2.5 kHz bandwidth [15] – the effects of which we include by convolving the simulated data with the CMUT impulse response prior to using our algorithm.

Finally, using our algorithm, we reconstruct the SoS distributions as shown in the middle column of Fig. 5 with root-mean-square (RMS) error of 9.7 m/s and 10 m/s, respectively which corresponds to only a minor variation in the soil moisture content [18]. While large lateral changes in SoS within the imaging window are challenging to reconstruct, subsequent spatially adjacent data captures could be independently reconstructed and stitched to form a continuous, large-scale reconstruction.

V. Conclusion

In this paper, we demonstrate a non-contact thermoacoustic soil moisture sensing approach that relies on the correlation between ultrasound wave speed and soil moisture content. An iterative speed-of-sound reconstruction algorithm was developed for the thermoacoustic sensing system, and simulation results show accurate reconstruction of the ground-truth speed-of-sound profiles. The hybrid nature of the proposed system provides multiple degrees of freedom in system design that help alleviate challenges in existing technologies and could permit non-invasive, below-ground sensing at scale.

Future work will include experimentally validating the simulation framework and results, incorporating the use of inherent soil heterogeneity or sub-surface structures, and mapping the reconstructed speed-of-sound profile to various true soil moisture distributions.

REFERENCES

[1] D. Hillel, *Soil in the environment: crucible of terrestrial life*. Elsevier, 2007.

[2] K. Noborio, "Measurement of soil water content and electrical conductivity by time domain reflectometry: a review," *Computers and electronics in agriculture*, vol. 31, no. 3, pp. 213–237, 2001.

[3] F. Kizito, C. S. Campbell, G. S. Campbell, D. R. Cobos, B. L. Teare, B. Carter, and J. W. Hopmans, "Frequency, electrical conductivity and temperature analysis of a low-cost capacitance soil moisture sensor," *Journal of Hydrology*, vol. 352, no. 3-4, pp. 367–378, 2008.

[4] D. Chanasyk and M. A. Naeth, "Field measurement of soil moisture using neutron probes," *Canadian Journal of Soil Science*, vol. 76, no. 3, pp. 317–323, 1996.

[5] P. Dobriyal, A. Qureshi, R. Badola, and S. A. Hussain, "A review of the methods available for estimating soil moisture and its implications for water resource management," *Journal of Hydrology*, vol. 458, pp. 110–117, 2012.

[6] Y. Y. Liu, W. A. Dorigo, R. Parinussa, R. A. de Jeu, W. Wagner, M. F. McCabe, J. Evans, and A. Van Dijk, "Trend-preserving blending of passive and active microwave soil moisture retrievals," *Remote Sensing of Environment*, vol. 123, pp. 280–297, 2012.

[7] D. Robinson, C. Campbell, J. Hopmans, B. K. Hornbuckle, S. B. Jones, R. Knight, F. Ogden, J. Selker, and O. Wendroth, "Soil moisture measurement for ecological and hydrological watershed-scale observatories: A review," *Vadose Zone Journal*, vol. 7, no. 1, pp. 358–389, 2008.

[8] A. Pohlmeier, A. Oros-Peusquens, M. Javaux, M. Menzel, J. Vanderborght, J. Kaffanke, S. Romanzetti, J. Lindenmair, H. Vereecken, and N. Shah, "Changes in soil water content resulting from ricinus root uptake monitored by magnetic resonance imaging," *Vadose zone journal*, vol. 7, no. 3, pp. 1010–1017, 2008.

[9] D. Dietrich, "Hydrotropism: how roots search for water," *Journal of experimental botany*, vol. 69, no. 11, pp. 2759–2771, 2018.

[10] Y. Bao, P. Aggarwal, N. E. Robbins, C. J. Sturrock, M. C. Thompson, H. Q. Tan, C. Tham, L. Duan, P. L. Rodriguez, T. Vernoux *et al.*, "Plant roots use a patterning mechanism to position lateral root branches toward available water," *Proceedings of the National Academy of Sciences*, vol. 111, no. 25, pp. 9319–9324, 2014.

[11] A. Singhvi, B. Ma, J. D. Scharwies, J. R. Dinneny, B. T. Khuri-Yakub, and A. Arbabian, "Non-contact thermoacoustic sensing and characterization of plant root traits," in *2019 IEEE International Ultrasonics Symposium (IUS)*. IEEE, 2019, pp. 1992–1995.

[12] H. Stoffregen, T. Zenker, and G. Wessolek, "Accuracy of soil water content measurements using ground penetrating radar: comparison of ground penetrating radar and lysimeter data," *Journal of Hydrology*, vol. 267, no. 3-4, pp. 201–206, 2002.

[13] I. Lunt, S. Hubbard, and Y. Rubin, "Soil moisture content estimation using ground-penetrating radar reflection data," *Journal of hydrology*, vol. 307, no. 1-4, pp. 254–269, 2005.

[14] J. A. Doolittle, F. E. Minzenmayer, S. W. Waltman, E. C. Benham, J. Tuttle, and S. Peaslee, "Ground-penetrating radar soil suitability map of the conterminous united states," *Geoderma*, vol. 141, no. 3-4, pp. 416–421, 2007.

[15] A. Singhvi, K. C. Boyle, M. Fallahpour, B. T. Khuri-Yakub, and A. Arbabian, "A microwave-induced thermoacoustic imaging system with non-contact ultrasound detection," *IEEE transactions on ultrasonics, ferroelectrics, and frequency control*, 2019.

[16] B. Ma, K. Firouzi, K. Brenner, and B. T. Khuri-Yakub, "Wide bandwidth and low driving voltage vented cmuts for airborne applications," *IEEE transactions on ultrasonics, ferroelectrics, and frequency control*, vol. 66, no. 11, pp. 1777–1785, 2019.

[17] W. Brutsaert and J. N. Luthin, "The velocity of sound in soils near the surface as a function of the moisture content," *Journal of Geophysical Research*, vol. 69, no. 4, pp. 643–652, 1964.

[18] F. Adamo, G. Andria, F. Attivissimo, and N. Giaquinto, "An acoustic method for soil moisture measurement," *IEEE transactions on instrumentation and measurement*, vol. 53, no. 4, pp. 891–898, 2004.

[19] M. Jaeger, G. Held, S. Peeters, S. Preisser, M. Grünig, and M. Frenz, "Computed ultrasound tomography in echo mode for imaging speed of sound using pulse-echo sonography: proof of principle," *Ultrasound in medicine & biology*, vol. 41, no. 1, pp. 235–250, 2015.

[20] R. Ali and J. J. Dahl, "Distributed phase aberration correction techniques based on local sound speed estimates," in *2018 IEEE International Ultrasonics Symposium (IUS)*. IEEE, 2018, pp. 1–4.

[21] C. Li, N. Duric, P. Littrup, and L. Huang, "In vivo breast sound-speed imaging with ultrasound tomography," *Ultrasound in medicine & biology*, vol. 35, no. 10, pp. 1615–1628, 2009.

[22] A. Hormati, I. Jovanović, O. Roy, and M. Vetterli, "Robust ultrasound travel-time tomography using the bent ray model," in *Medical Imaging 2010: Ultrasonic Imaging, Tomography, and Therapy*, vol. 7629. International Society for Optics and Photonics, 2010, p. 76290I.

[23] Y. Quan and L. Huang, "Sound-speed tomography using first-arrival transmission ultrasound for a ring array," in *Medical Imaging 2007: Ultrasonic Imaging and Signal Processing*, vol. 6513. International Society for Optics and Photonics, 2007, p. 651306.

[24] X. Qu, T. Azuma, H. Lin, H. Imoto, S. Tamano, S. Takagi, S.-i. Umemura, I. Sakuma, and Y. Matsumoto, "Phase aberration correction by multi-stencils fast marching method using sound speed image in ultrasound computed tomography," in *Medical Imaging 2016: Ultrasonic Imaging and Tomography*, vol. 9790. International Society for Optics and Photonics, 2016, p. 979018.

[25] J. Hsieh, *Computed tomography: principles, design, artifacts, and recent advances*. SPIE press, 2003, vol. 114.

[26] R. Mallart and M. Fink, "Adaptive focusing in scattering media through sound-speed inhomogeneities: The van cittert zernike approach and focusing criterion," *The Journal of the Acoustical Society of America*, vol. 96, no. 6, pp. 3721–3732, 1994.

[27] R. Ali and J. J. Dahl, "Travel-time tomography for local sound speed reconstruction using average sound speeds," in *2019 IEEE International Ultrasonics Symposium (IUS)*. IEEE, 2019, pp. 2007–2010.

[28] P. Filippi, A. Bergassoli, D. Habault, and J. P. Lefebvre, *Acoustics: basic physics, theory, and methods*. Elsevier, 1998.

[29] J. A. Sethian, "Fast marching methods," *SIAM review*, vol. 41, no. 2, pp. 199–235, 1999.

[30] S. Boyd, N. Parikh, E. Chu, B. Peleato, J. Eckstein *et al.*, "Distributed optimization and statistical learning via the alternating direction method of multipliers," *Foundations and Trends® in Machine learning*, vol. 3, no. 1, pp. 1–122, 2011.

[31] C. C. Paige and M. A. Saunders, "Lsqr: An algorithm for sparse linear equations and sparse least squares," *ACM Transactions on Mathematical Software (TOMS)*, vol. 8, no. 1, pp. 43–71, 1982.

[32] B. E. Treeby and B. T. Cox, "k-wave: Matlab toolbox for the simulation and reconstruction of photoacoustic wave fields," *Journal of biomedical optics*, vol. 15, no. 2, p. 021314, 2010.